Domain wall motion in nanowires using moving grids (invited)

H. Forster,[a] T. Schrefl, D. Suess, W. Scholz, V. Tsiantos, R. Dittrich, and J. Fidler
Institute for Applied and Technical Physics, Vienna University of Technology, Wiedner Hauptstraße 8-10/137, A-1040 Vienna, Austria

The magnetization reversal process of Co nanowires was investigated using a moving mesh technique. The nucleation and expansion of reversed domains is calculated by solving the Gilbert equation of motion for different damping constants. The adaptive finite element method reduces the total CPU time by more than a factor of 4 as compared to a uniform mesh. Two different domain wall types are observed. For a wire diameter of $d=10$ nm transverse walls occur and gyromagnetic precession limits the domain wall velocity. The domain wall velocity increases from 50 to 520 m/s as the Gilbert damping constant increases from $\alpha=0.05$ to $\alpha=1$ at an applied field of 500 kA/m. For a diameter greater than 20 nm vortex walls are formed. The vortex mobility increases with decreasing damping constant. Thus velocities up to 2000 m/s are reached for a wire diameter of 40 nm, $\alpha=0.05$, and an applied field of 250 kA/m. © *2002 American Institute of Physics.*
[DOI: 10.1063/1.1452189]

I. INTRODUCTION

Magnetic nanowires are of great practical and theoretical interest. Future magneto-electronic devices and magnetic sensors may be based on the magnetoresistance of domain walls moving in nanowires. Lee and co-workers[1] investigated the nucleation of domain walls in NiFe wire junctions using a magnetic force microscopy and micromagnetic calculations. Domain walls nucleate in the wider part and are trapped in the junction area. Based on these results the authors suggest structures which may be used to launch domain walls into wires with a controlled external field. Ono and co-workers[2] investigated magnetization reversal in NiFe/Cu/NiFe trilayers using the giant magnetoresistance effect. The time variation of the resistance was measured to estimate the domain wall velocity. Taniyama and co-workers[3] reported a negative magnetoresistance due to domain walls in Co zigzag wires. McMichael and co-workers[4] used micromagnetic simulations to investigate the motion of transverse head-to-head walls within a domain wall trap consisting of a shaped NiFe wire with two wide ends. The influence of Bloch lines and vortices on domain wall motion in prismatic wires was investigated by Nakatani and co-workers.[5] They calculated the domain wall velocity as a function of the wire dimensions by solving the Landau–Lifshitz–Gilbert equation. The possible wall structures of head-to-head walls in thin Permalloy films were numerically computed by McMichael.[6]

This work uses an adaptive finite element technique to calculate the domain wall motion in cylindrical Co nanowires. The number of finite elements remains small while it is also possible to resolve the micromagnetic details of the reversal process. Miltat[7] analyzed two-dimensional Néel-type walls, using a discretization of the sample into rectangular prisms of variable size having small elements in the center of the wall. Tako[8] introduced *a posteriori* refinement which subdivides triangular elements with large errors into four smaller elements. Hertel and Kronmüller applied an adaptive finite element method to calculate domain configurations and vortex motion in thin film elements.[9] In this work, mesh refinement and mesh coarsening is applied, in order to obtain a high density mesh which moves together with the domain wall. The magnetostatic fields are calculated using a hybrid finite element/boundary element method. The domain wall velocity is calculated numerically as a function of the external field, the wire diameter, and the Gilbert damping constant. The results show that the characteristics of the domain wall change significantly depending on the diameter of the nanowire. The domain wall velocity strongly depends on the external field and the damping constant α. Section II presents the micromagnetics formalism followed by Sec. III explaining the adaptive finite element method used for the calculations. Section IV treats the influence of the wall structure on the domain wall velocity.

II. MICROMAGNETICS

Micromagnetics is a continuum theory for the description of magnetization processes in ferromagnetic materials. The theory starts from the total magnetic Gibbs free energy. The competitive effects of the micromagnetic energy contributions upon minimization of the free energy determine the equilibrium distribution of the magnetization. In the presented simulations four energies are considered: the exchange energy, the anisotropy energy, the Zeeman energy, and the magnetostatic energy which favors the creation of magnetic domains. So we neglect magnetostriction and surface anisotropy. The total magnetic Gibbs free energy can be written as follows:[10]

$$E_t = \int \left[A \sum_{i=1}^{3} (\nabla \beta_i)^2 - K_u (\mathbf{u}\cdot\beta)^2 - \frac{1}{2}\mathbf{J}\cdot\mathbf{H}_d - \mathbf{J}\cdot\mathbf{H}_{ext} \right] dV, \quad (1)$$

where A is the exchange constant, β_i denotes the direction cosines of the magnetic polarization vector, **J**

[a]Electronic mail: hermann.forster@tuwien.ac.at

$=(\beta_1,\beta_2,\beta_3)J_s$. K_u and $\mathbf{u}$ are the magneto-crystalline anisotropy constant and the anisotropy direction. $\mathbf{H}_{ext}$ is the external field. The demagnetizing field, $\mathbf{H}_d$, follows from a magnetic scalar potential. The magnetic scalar potential solves the magnetostatic boundary value problem and can be effectively computed using a hybrid finite element/boundary element method.[11]

The actual path that the system follows towards a local minimum is obtained from the time integration of the Gilbert equation of motion[12]

$$\frac{\partial \mathbf{J}}{\partial t} = -|\gamma| \mathbf{J} \times \mathbf{H}_{eff} + \frac{\alpha}{J_s} \mathbf{J} \times \frac{\partial \mathbf{J}}{\partial t}. \tag{2}$$

The effective field $\mathbf{H}_{eff}$, which provides the torque acting on the magnetization, is the negative variational derivative of the magnetic Gibbs free energy, $\mathbf{H}_{eff} = -\delta E_T / \delta \mathbf{J}$. The first term describes the dyromagnetic precession, where γ is the gyromagnetic ratio. The second term describes the damping which is characterized by the Gilbert damping constant α. In equilibrium the torque, $\mathbf{J} \times \mathbf{H}_{eff}$, vanishes and the magnetic polarization is at rest.

III. ADAPTIVE FINITE ELEMENT METHOD

To solve the partial differential equations we use the finite element method. The magnetic wire is divided into tetrahedral finite elements. Within each element the direction cosines β_i are interpolated by a linear function. The space discretization leads to a system of coupled magnetic moments sitting at the nodes of the finite element mesh. The effective field at the nodes follows from the derivative of the Gibbs free energy with respect to the magnetic moment. The Gilbert equation of motion (2) has to be solved for each magnetic moment. The equations are coupled by the exchange and magnetostatic interactions between the magnetic moments. The time integration is performed using the software package CVODE.[13] The details of the time integration are described elsewhere.[14] The backward differentiation method was found to require less CPU time than the Adams method.

In order to resolve a magnetic domain wall the element size has to be smaller than the characteristic length, l_c, given by the minimum of the exchange length l_{ex} and the Bloch parameter δ_0

$$l_c = \min(l_{ex}, \delta_0) = \min\left(\sqrt{\frac{2\mu_0 A}{J_S^2}}, \sqrt{\frac{A}{K_u}} \right). \tag{3}$$

If the element size is too big a so-called domain wall collapse[15] will occur: the magnetization becomes aligned antiparallel at neighboring nodes and the torque on the magnetization vanishes. A large number of finite elements is required for the study of wall motion in magnetic wires using a uniform fine grid with an element size $h \leqslant l_c$. In order to keep the number of finite elements small and avoid the domain wall collapse, an adaptive refinement scheme can be applied.

The outline of adaptive algorithms is as follows. Starting from an initial finite element mesh τ_0, we produce a sequence of refined grids τ_m, until the estimated error is below a given tolerance ϵ. Generally we have to distinguish three refinement strategies.[16] First there is the possibility of moving the nodes from positions with nearly uniform magnetization to the wall or vortices regions (*r*-refinement). Then there is the possibility of adding new nodes and elements into the elements having a big error indicator (*h*-refinement). The third way is to interpolate the direction cosines β_i by polynomials of higher order instead of linear functions (*p*-refinement). The aim of an adaptive refinement algorithm is to get the ''optimal'' mesh, where the number of nodes is as small as possible while keeping the error below a given tolerance. All strategies are based on the idea of an equidistribution of the local error indicator to all mesh elements. Babuska and Rheinboldt[17] state that a mesh is almost optimal when the local errors are approximately equal for all elements. Adaptive mesh algorithms have to identify the regions where a higher spatial resolution is required. Therefore so-called error indicators are computed from the current finite element solution. in micromagnetics a reliable error indicator is based on the constraint condition for the norm of the magnetization vector.[18] Strong deviations of the norm show regions with nonuniform magnetization.[19] Figure 1 shows this error indicator for subsequent meshes during *h*-refinement. We assume an existing domain wall in the Conanowire. Dark regions correspond to a high error indicator. Each plot corresponds to one refinement step. From left to right the decreasing error indicator with increasing number of elements is visible. So with each iteration the condition of Babuska and Reinboldt is met in a better way.

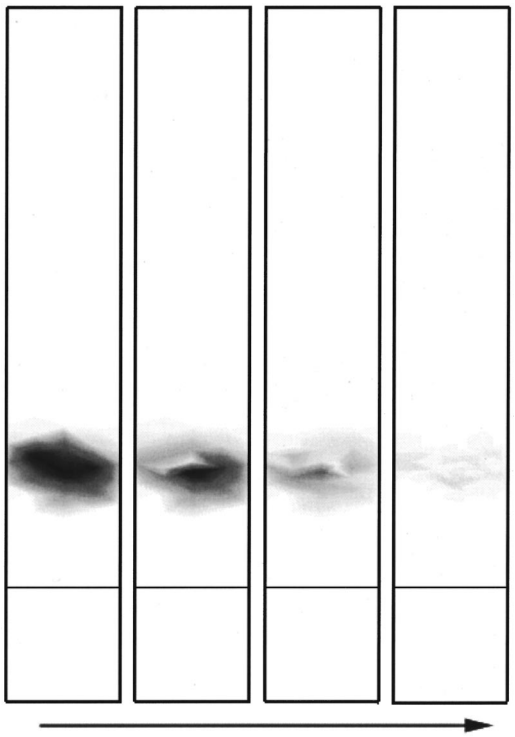

FIG. 1. Sequence of snapshots of the error indicator with an existing domain wall. Dark regions correspond to a high error indicator. Each plot corresponds to one refinement step.

In the following we outline the *h*-refinement scheme used in the micromagnetic simulations of domain wall mo-

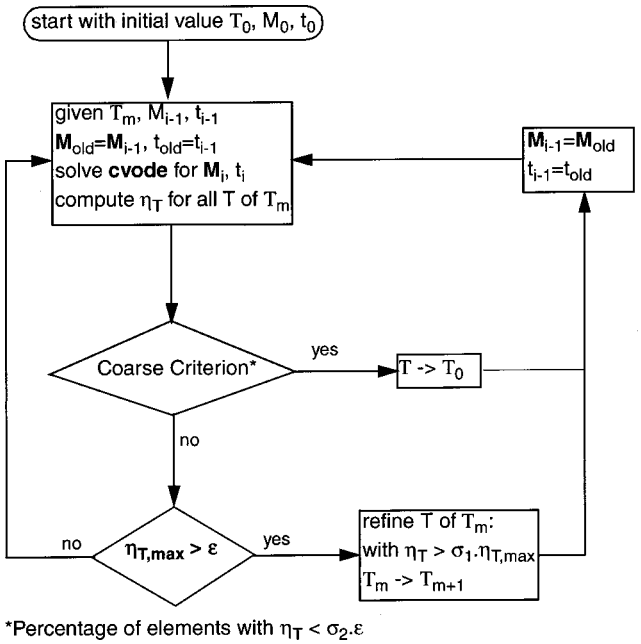

FIG. 2. Flow chart of the adaptive mesh micromagnetic algorithm. The simulation proceeds in time only if the space discretization error is below a certain threshold ϵ.

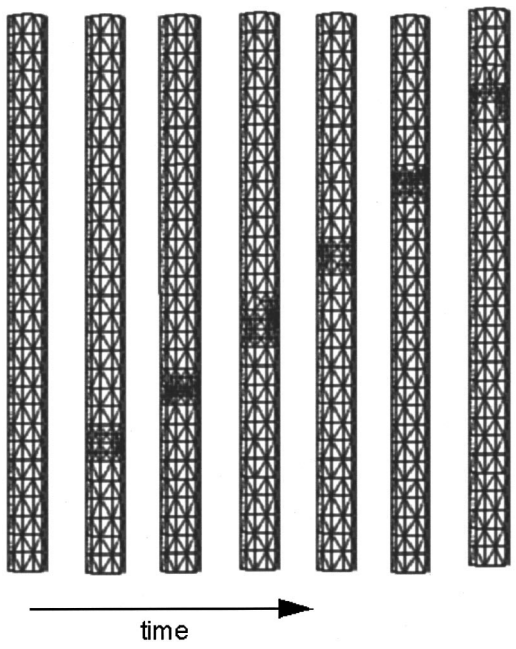

FIG. 3. Sequence of meshes during the motion of the domain wall. The pictures give the triangular mesh on the surface of the wire.

tion. The finite element grid is adjusted to the current wall position during the solution of the Gilbert equation of motion. The mesh is refined in regions with nonuniform magnetization, whereas elements are taken out where the magnetization is uniform. Thus the fine grid moves together with the wall, as the mesh can be coarsened as soon as the wall has passed by.

Figure 2 shows the flow chart of the corresponding algorithm: We start with the initial mesh τ_0, initial magnetization $\mathbf{M_0}$ and the starting time t_0. At each time step i CVODE integrates the Gilbert equation of motion [Eq. (2)] and gives the new values for the magnetization $\mathbf{M}_i$ at time t_i. Furthermore, the error indicator η_T for all elements T of the given mesh τ_m is calculated. We control the adaptive refinement method with σ_1, σ_2 and a certain threshold value ϵ, which represents the allowed error.

Through proper refinement and coarsening steps we obtain a mesh with the error indicator η_T for all elements. First we treat the question, if coarsening of the current mesh is possible: Is the percentage of elements, which fulfill $\eta_T < \sigma_2 \cdot \epsilon$, higher than a given value (coarse criterion)? Then there are regions, which just require a coarser mesh. So we can go back to the initial mesh τ_0 and subsequently refine the mesh in regions with high error indicators.

The other possibility is that we cannot coarse our mesh. Then we must decide, if the mesh has to be refined. The condition is: If there are elements with $\eta_T > \epsilon$, then a refinement process[20] is required. We refine all elements whose error indicator fulfills $\eta_T > \sigma_1 \cdot \epsilon$, with $\sigma_1 \in (0,1)$.[21] The algorithm leads to the new mesh τ_{m+1}. If the directions of the magnetization differ very much between neighboring elements and more than one refinement step is required to reduce the error indicator in a significant number of elements, then the refinement steps are repeated. Since a system of coupled equations has to be solved in every iteration of this algorithm, the number of iterations should be as small as possible. Thus, the marking strategy should select not too few mesh elements for refinement in each cycle. Therefore, not just elements with $\eta_T < \epsilon$ are marked for refinement, but in addition all elements fulfilling $\eta_T < \sigma_1 \cdot \epsilon$.

In both cases the saved magnetization $\mathbf{M}_{old}$ of the former time step is interpolated on the currently active mesh and the time is set to the former value t_{old}. This means: If the error is too large or if the mesh can be coarsened the time step is rejected and the finite element mesh is adjusted.

Otherwise, if the mesh cannot be coarsened or does not have to be refined, the time integration is continued on the given grid. Thus the simulation proceeds in time only if the space discretization error is below a certain threshold.

Numerical studies[22] showed that the moving mesh reduces the total CPU time by more than a factor of 4. Figure 3 shows a sequence of grids during the simulation of domain wall motion in a Co wire. The mesh size in the coarse region is 20 nm, whereas the mesh size at the wall position approaches l_c, which is 4.3 nm for the investigated Co wire.

IV. RESULTS AND DISCUSSION

Figure 4 shows the model of the simulated geometry. The magnetic Co nanowire has a total length of 600 nm. The nanowire has two stable states: all magnetic moments are parallel to the long axis, pointing either in one direction or in the other. We apply an external field parallel to the long axis in the opposite direction of the magnetization. If the field is large enough, a reversed domain will be formed, a head-to-head domain wall will be built and will propagate through the whole nanowire, until it arrives at the other end. There it is annihilated, leaving the system in the second possible stable state. Since the aim of this work is to investigate the

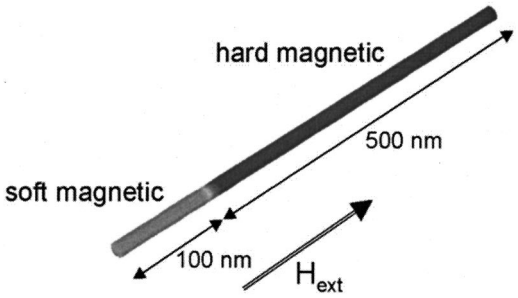

FIG. 4. Finite element model of the two-phase wire. The total length of the nanowire is 600 nm. The soft magnetic part with zero anisotropy facilitates the nucleation of reversed domains. The hard magnetic part has the material parameters of Co (spontaneous magnetic polarization $J_S = 1.76$ T, exchange constant $A = 1.3 \times 10^{-11}$ J/m, and the magneto-crystalline anisotropy parallel to the long axis, $K_u = 4.5 \times 10^5$ J/m^3).

propagation of a domain wall through the nanowire, we have to control the nucleation of the reversed domain. Therefore, we divide the wire into two parts. One hard magnetic part of 500 nm length having uniaxial anisotropy parallel to the long axis and a short end (100 nm) with zero magneto-crystalline anisotropy. The material parameters are $J_s = 1.76$ T, $A = 1.3 \times 10^{-11}$ J/m, and $K_u = 4.5 \times 10^5$ J/m^3.[23] Under the influence of an opposing field the nucleation of a reversed domain is formed in the soft magnetic part because of the lower domain wall energy in the soft magnetic end. Then we observe the propagation of the domain wall in the hard magnetic part.

Figure 5 shows that the magnetic polarization J parallel to the long axis as a function of time decreases linearly. We

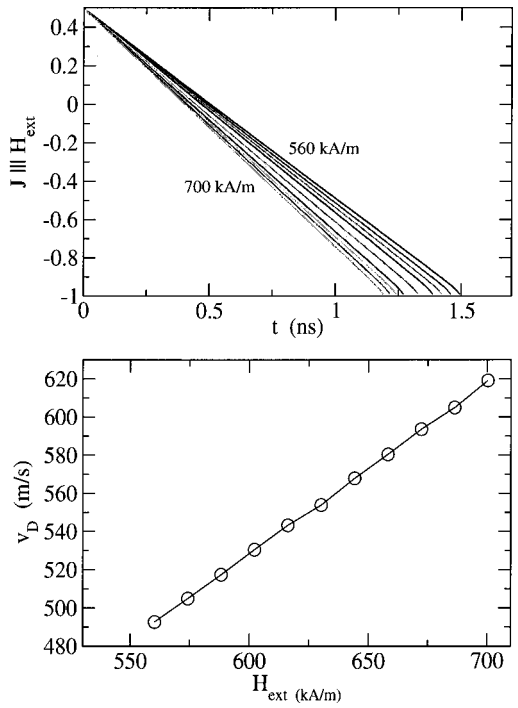

FIG. 5. Calculation of the domain wall velocity. Top: Total magnetic polarization parallel to the long axis for different applied fields. The different lines refer to different fields in the range from 560 to 700 kA/m with a step of 14 kA/m. Bottom: Domain wall velocity as a function of the applied field. The wire diameter is $d = 10$ nm and the Gilbert damping constant $\alpha = 1$.

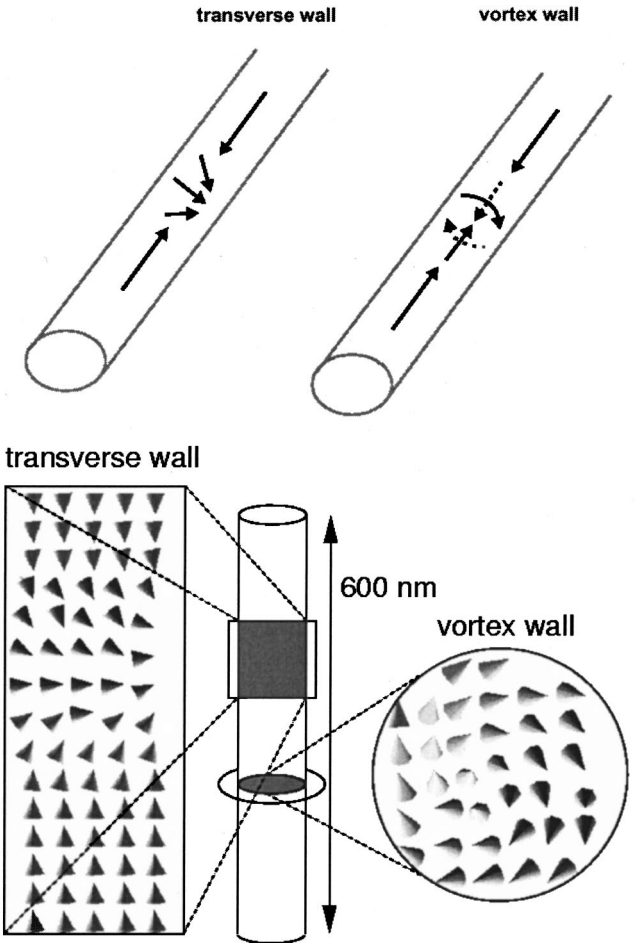

FIG. 6. Above: Schematics of the magnetization in the transverse wall and in the vortex wall. Bottom: Magnetization distribution in a transverse wall (cut plane parallel to the wire axis) and in a vortex wall (cut plane perpendicular to the wire axis through the vortex core). The wire diameter $d = 20$ nm and the Gilbert damping constant $\alpha = 1$.

obtain the domain wall velocity as a function of the applied field H_{ext} from the slope of the curves, dJ/dt.

We found that the domain wall velocity and the structure of the domain wall strongly depend on the diameter d of the nanowire. Two types of domain walls can be formed. Figure 6 shows the structure of the so-called transverse wall and the structure of the vortex wall during their motion through the nanowire. In the first case the magnetization in the center of the wall points perpendicular to the long axis of the wire. As the wall moves, the transverse component of the magnetization circles around driven by gyromagnetic precession.[24] In the second case a vortex is formed in a plane normal to the long axis of the wire. The magnetization aligns parallel to the wire surface. Within the domain wall the magnetization rotates around the long axis which leads to the formation of a Bloch point in the middle of the wire. The formation of the vortex decreases the magnetostatic energy at the expense of the exchange energy. For small diameters, it is energetically preferable to form a transverse wall which minimizes the exchange energy due to the parallel alignment of the magnetization in the domain wall. On the other hand, there are no flux closure states in the wire and so the magnetostatic energy is not reduced. However, for small diameters, the ex-

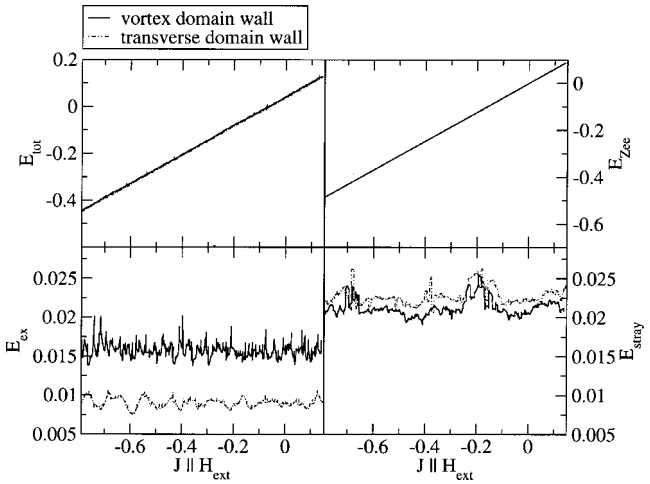

FIG. 7. Energy contributions for a vortex and a transverse domain wall at a diameter $d=20$ nm, an applied field $H_{ext}=490$ kA/m, and a damping constant $\alpha=1$. $J\|H_{ext}$ represents the time evolution of the simulation.

change energy is the most dominant energy contribution to the total Gibbs free energy, and so its minimization determines the wall configuration. With increasing diameter the magnetostatic energy becomes more important in the minimization process. Although the vortex wall increases the exchange energy, the minimization of the magnetostatic energy due to the lower demagnetizing field makes it energetically preferable. Figure 7 compares the two energy contributions. Since the difference in the total Gibbs free energy is less than 1% at a critical diameter of $d=20$ nm, it is possible to obtain both domain wall structures. We clearly see the lower exchange energy E_{ex} of the transverse domain wall and the decrease in stray field energy E_{stray} if we switch to the vortex wall structure. For $d<20$ nm only transverse walls are observed and for $d>20$ nm only vortex walls are observed. Figure 8 gives the wall velocities for different wire diameters. The two sets of data for $d=20$ nm refer to the transverse wall (open symbols) and the vortex wall (filled symbols).

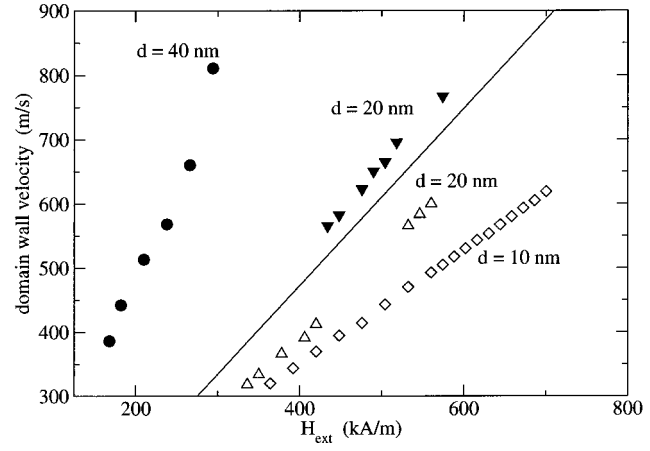

FIG. 8. Domain wall velocity as a function of the applied field for different wire diameters. The open symbols and the filled symbols refer to transverse and vortex walls, respectively.

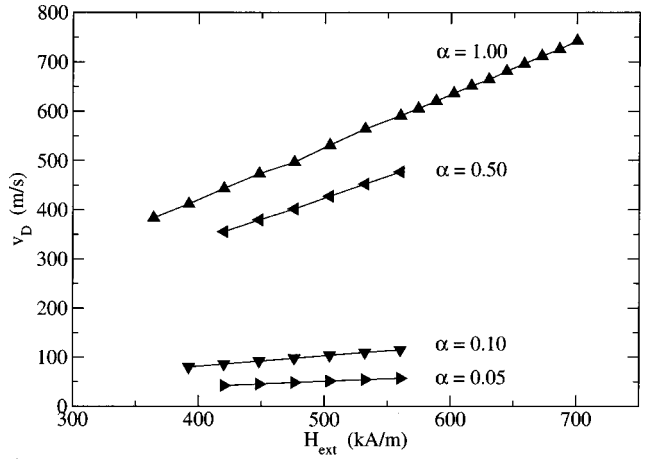

FIG. 9. Domain wall velocity of transverse walls for different damping constants. The wire diameter is $d=10$ nm.

The dependence on the damping constant α is not the same for both structures. For $d=10$ nm just transverse walls are formed. Figure 9 shows the domain wall velocities. With increasing damping constant the velocity increases from 50 m/s for $\alpha=0.05$ to 520 m/s for $\alpha=1$ at an applied field of 500 kA/m. For higher damping constants the domain wall velocity increases faster for higher external fields. In the transverse wall gyromagnetic precession plays a major role during the wall motion. Figure 10 shows the domain wall velocity for a diameter of 40 nm. In this case only vortex walls are formed. On the contrary, for the vortex walls the domain wall velocity increases with decreasing damping constant, reaching 2000 m/s for $d=40$ nm, $\alpha=0.05$, and an applied field of 250 kA/m.

The analysis of the micromagnetic results shows that during wall motion the center of the vortex does not remain in the middle of the wire. The vortex core moves towards the surface, where it is annihilated. Since this configuration is energetically not favorable, a new vortex forms, which moves towards the opposite side. This process is repeated periodically. The observed increase of the vortex domain wall velocity with decreasing damping constant is expected in Bloch-type walls.[25] Obviously vortex walls give higher

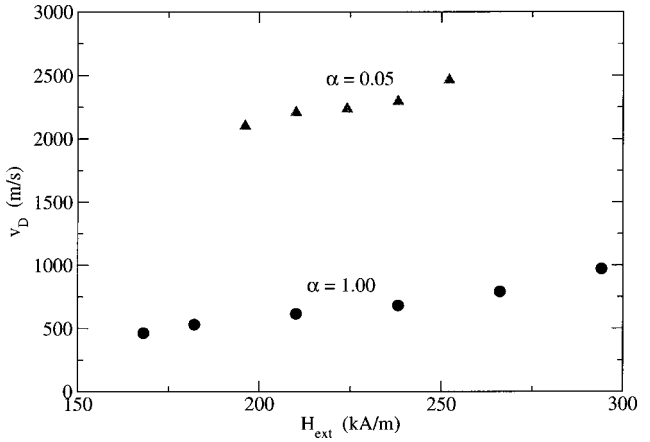

FIG. 10. Domain wall velocity of vortex walls for different damping constants. Triangles $\alpha=0.05$; circles: $\alpha=1$. The wire diameter is 40 nm.

velocities than transverse walls due to the more Bloch-like character leading to a higher mobility of the wall.[26]

V. CONCLUSIONS

Numerical micromagnetic calculations have been carried out to investigate the propagation of a domain wall in a Co nanowire. To increase the efficiency of our calculations we have introduced an adaptive mesh algorithm. With this feature we had the possibility of investigating bigger problems in shorter times. We reduced the computation time by a factor of 4.

The simulations show that the domain wall velocity in magnetic nanowires significantly depends on different parameters. For a wire diameter $d<20$ nm just transverse walls are formed and for $d>20$ nm vortex walls are formed. For $d=20$ nm the energy of the transverse and the vortex walls is rather similar. Depending on the applied field during the nucleation process, either one of the two walls can be formed. The velocity of a vortex wall is about 1.3 times higher than the wall velocity of the transverse wall.

ACKNOWLEDGMENT

This work was supported by the Austrian Science Fund (Y132-PHY).

[1] W. Y. Lee, C. C. Yao, A. Hirohata, Y. B. Xu, H. T. Leung, S. M. Gardiner, S. McPhail, B. C. Choi, D. G. Hasko, and J. A. C. Bland, J. Appl. Phys. **87**, 3032 (2000).
[2] T. Ono, H. Miyajima, K. Shigeto, K. Mibu, N. Hosoito, and T. Shinjo, J. Appl. Phys. **85**, 6181 (1999).
[3] T. Taniyama, I. Nakatani, T. Namikawa, and Y. Yamazaki, Phys. Rev. Lett. **82**, 2780 (1999).
[4] R. D. McMichael, J. Eicke, M. J. Donahue, and D. G. Porter, J. Appl. Phys. **87**, 7058 (2000).
[5] Y. Nakatani, N. Hayashi, T. Ono, and H. Miyajima, IEEE Trans. Magn., **37**, 2129 (2001).
[6] R. D. McMichael and M. J. Donahue, IEEE Trans. Magn. **33**, 4167 (1997).
[7] J. Miltat and M. Labrune, IEEE Trans. Magn. **30**, 4350 (1994).
[8] K. M. Tako, T. Schrefl, M. A. Wongsam, and R. W. Chantrell, J. Appl. Phys. **81**, 4082 (1997).
[9] R. Hertel and H. Kronmüller, IEEE Trans. Magn. **34**, 3922 (1998).
[10] W. F. Brown, Phys. Rev. **130**, 1677 (1963).
[11] D. R. Fredkin and T. R. Koehler, IEEE Trans. Magn. **26**, 415 (1990).
[12] T. L. Gilbert, Phys. Rev. **100**, 1243 (1955).
[13] S. D. Cohen and A. C. Hindmarsh, Comput. Phys. **10**, 138 (1996).
[14] D. Suess, V. Tsiantos, T. Schrefl, J. Fidler, W. Scholz, H. Forster, and R. Dittrich, J. Magn. Magn. Mater. (submitted).
[15] M. Donahue, J. Appl. Phys. **83**, 6491 (1998).
[16] A. Raizer, S. R. H. Hoole, G. Meunier, and J.-L. Coulomb, J. Appl. Phys. **67**, 5803 (1990).
[17] I. Babuska and W. Rheinboldt, SIAM (Soc. Ind. Appl. Math.) J. Numer. Anal. **15**, 736 (1978).
[18] W. Scholz, T. Schrefl, and J. Fidler, J. Magn. Magn. Mater. **196-197**, 933 (1999).
[19] A. Bagnérés-Viallix, P. Baras, and J. B. Albertini, IEEE Trans. Magn. **27**, 3819 (1991).
[20] H. P. Langtangen, *Computational Partial Differential Equations - Numerical Methods and Diffpack Programming* (Springer, New York, 1999).
[21] A. Schmidt and K. G.Siebert, "Numerical aspects of parabolic freeboundary problems-Adaptive finite element methods." URL: http://www.mathematik.uni-freiburg.de/ IAM/homepages/alfred/notesjyv.html
[22] T. Schrefl, H. Forster, D. Suess, W. Scholz, V. Tsiantos, and J. Fidler, *Advances in Solid State Physics* (Springer, Berlin, 2001), in press.
[23] W. Yang, J. Appl. Phys. **87**, 6884 (2000).
[24] R. Hertel, J. Magn. Magn. Mater. (in press).
[25] W. Doering, J. Appl. Phys. **39**, 1006 (1968).
[26] K. J. Kirk, M. R. Scheinfein, J. N. Chapman, S. McVitie, M. F. Gillies, B. R. Ward, and J. G. Tennant, J. Phys. D **34**, 160 (2001).